

# 17 and 34 GHz Observations of the Sun with the Nobeyama Radioheliograph

Ken'ichi FUJIKI

*Solar-Terrestrial Environment Laboratory, Nagoya University, Toyokawa, Aichi 442-8507, Japan*

*E-mail: fujiki@stelab.nagoya-u.ac.jp*

## Abstract

Since the beginning of dual-frequency observations with the Nobeyama Radioheliograph, many flares and related energetic phenomena have been observed. Some of them are sufficiently intense in microwave and mm-wave ranges that it is possible to synthesize 34 GHz images together with the corresponding 17 GHz images. Dual-frequency analyses of them provide us with spectral information which reflects physical conditions in flare regions such as energy distribution of high-energy electrons, magnetic fields, and density of heated plasmas.

In this paper, we briefly present observations of two flares and a prominence eruption which were obtained by the Nobeyama Radioheliograph at 17 and 34 GHz.

**Key words:** Sun:flare — Sun:prominence — Sun:microwave and mm-wave

## 1. Introduction

The Nobeyama radioheliograph (NoRH) is a radio interferometer dedicated to solar observation. Routine observations at 17 GHz started in late June, 1992 (Nakajima et al. 1992). It was upgraded to a dual-frequency system at 17 and 34 GHz using a time-sharing system in late October 1995 (Takano et al. 1997).

Since each element antenna (80 cm diameter) covers the whole Sun and each pair of antennas measures a complex Fourier component of the brightness distribution of the Sun, full-sun images are obtained through an inverse Fourier transformation of the measured Fourier components. However, because the angular scale sampled by the shortest antenna spacing does not cover the whole sun at 34 GHz, aliasing patterns appear in the restored image. Nevertheless, the NoRH provides high quality images of radio sources if they are sufficiently brighter than other sources on the Sun. The spatial resolutions are moderately high,  $\sim 10''$  at 17 GHz and  $\sim 5''$  at 34 GHz, with a temporal resolution of 100 m sec at both frequencies. The dynamic ranges of 17 and 34 GHz images are 26 dB (Koshiishi et al, 1994) and 20 dB, respectively, in the case of flare observations, and 300 K (Koshiishi, 1996) and a few thousands K (not evaluated yet), respectively, in the case of observations of quiet regions.

The microwave and mm-wave spectrum derived from observations of solar flares at both frequencies provides an important constraint for an energy distribution of accelerated electrons, which is important for revealing acceleration mechanisms in solar flares. Since most spectra which have been observed so far do not contain spatial information, the spatially-resolved microwave and mm-wave spectrum observed with NoRH is quite useful for this type of study.

A few tens of flares and prominence eruptions have been observed with the NoRH since dual-frequency observations began in October, 1995. The NoRH is expected to be used for various solar studies in the next solar maximum. In this paper, I report some examples of dual-frequency observations with NoRH.

## 2. Observations

Events which have been observed since late October, 1995, are listed in Table 1. These events have large correlation coefficients at higher ( $>30$  arcmin) spatial frequencies at 17 GHz, and so high quality images are expected to be synthesized at both frequencies. Some of them are briefly described as examples in the following sub-sections.

Table 1.. Event list of flares. Events are selected by maximum correlation coefficient  $> 1.5 \times 10^{-2}$  since October 1995.

Date	Peak Time	Correlation Coefficient*	Date	Peak Time	Correlation Coefficient*
1996-04-22	03:36:15	$2.1 \times 10^{-2}$	1998-05-29	00:56:29	$3.5 \times 10^{-2}$
1997-08-26	00:53:40	$4.2 \times 10^{-2}$	1998-06-13	04:18:36	$5.1 \times 10^{-2}$
1997-09-22	00:48:30	$8.5 \times 10^{-2}$	1998-07-13	03:38:10	$2.2 \times 10^{-2}$
1997-09-24	02:47:09	$8.2 \times 10^{-2}$	1998-08-08	03:15:30	$3.7 \times 10^{-1}$
1997-09-24	05:34:18	$3.0 \times 10^{-2}$	1998-08-08	03:15:51	$1.9 \times 10^{-1}$
1997-11-04	02:35:09	$4.4 \times 10^{-2}$	1998-08-18	04:11:50	$5.2 \times 10^{-2}$
1997-11-29	22:40:19	$4.4 \times 10^{-2}$	1998-08-18	23:00:06	$3.8 \times 10^{-2}$
1998-03-19	01:26:11	$2.0 \times 10^{-2}$	1998-08-21	00:01:53	$2.9 \times 10^{-2}$
1998-03-20	04:44:52	$3.2 \times 10^{-2}$	1998-09-06	02:12:28	$2.6 \times 10^{-2}$
1998-04-23	05:41:39	$2.1 \times 10^{-1}$	1998-09-09	04:56:35	$4.1 \times 10^{-2}$
1998-05-02	04:57:25	$1.7 \times 10^{-2}$	1998-09-27	23:40:08	$4.2 \times 10^{-2}$
1998-05-05	05:29:25	$1.6 \times 10^{-2}$	1998-11-05	06:14:46	$1.6 \times 10^{-2}$
1998-05-05	23:04:05	$1.7 \times 10^{-2}$	1998-11-08	22:55:18	$2.4 \times 10^{-2}$
1998-05-06	04:00:40	$3.8 \times 10^{-2}$	1998-11-10	00:12:25	$4.6 \times 10^{-2}$
1998-05-06	04:55:14	$3.1 \times 10^{-2}$	1998-11-11	00:50:11	$2.2 \times 10^{-2}$
1998-05-08	01:57:55	$1.9 \times 10^{-2}$	1998-11-12	05:27:05	$1.3 \times 10^{-1}$
1998-05-08	06:00:34	$6.5 \times 10^{-2}$			

\*: Correlation coefficient at 17 GHz

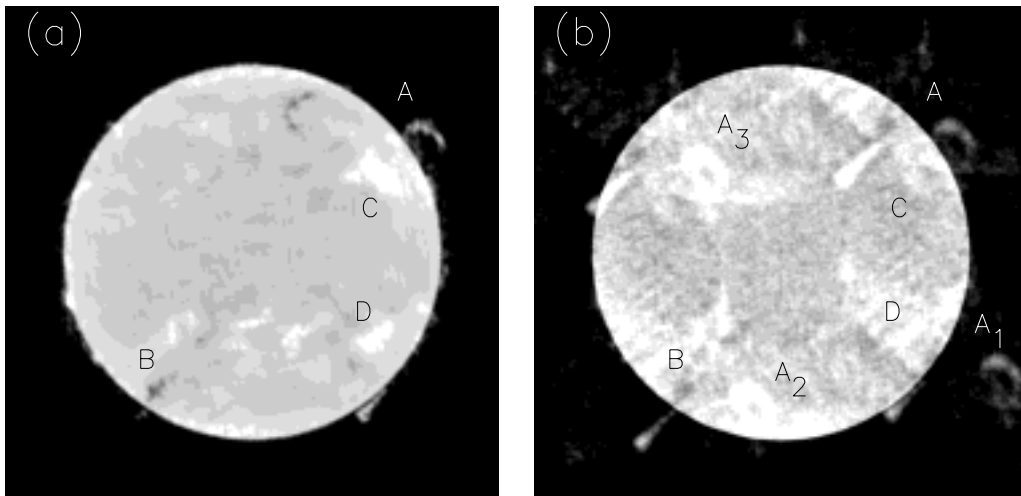


Fig. 1.. Full sun images at (a)17 and (b)34 GHz.

### 2.1. Full Sun Image

The first example is a full Sun image which was observed on 21 May, 1998, as shown in Fig. 1.

A prominence, a dark filament, and two active regions are marked with A, B, C, and D respectively. The prominence (A) is observed clearly at both frequencies but other structure marked B ~ D are not clearly seen.

As mentioned in the introduction, an aliasing pattern which can not be distinguished from real structure appears in the 34 GHz image. This pattern changes time by time because of projection effect of the solar image onto the antenna plane. The marks  $A_1 \sim A_3$ , in Fig. 1(b), are aliasing structures of A. Other aliasing patterns also appear on the image.

The size of the radio disk at both frequencies is assumed to be the same (1.0125 % larger than optical solar disk) because the sizes of dirty disks have no significant difference between these frequencies. The brightness temperature of solar disk at both frequencies are 10690 K and 9800 K, respectively, which are estimated from single dish observations by Zirin et al (1991), Linsky (1973), and Kuseski and Swanson (1976). The brightness temperature of the solar disk is normalized to  $1 \times 10^4$ K at both frequencies in the imaging process.

The spatial resolution at 34 GHz is two times better than that at 17 GHz. This can be seen when we compare the edges of the radio solar images at both frequencies. However, weak structures, which are observed to scatter on the 34 GHz solar image, seem to have a lower spatial resolution than those on the 17 GHz solar images, because weak structures at 34 GHz are not deconvolved in the imaging process. Note that sizes of the dirty beams, which are used in the 17 and 34 GHz imaging processes, are more than two times larger than the corresponding CLEAN beams. It is necessary to consider the beam dilution effects when we analyze weak structures.

It is clearly seen that the noise level at 34 GHz is larger than that at 17 GHz when the sky levels are compared. The patterns outside the radio Sun at 34 GHz is superposition of error sidelobes and higher random noise than at 17 GHz. The complex aliasing pattern due to the lack of the fundamental spatial frequency often complicates the imaging process at 34 GHz. In such cases, the error sidelobes increase markedly. Modifications to the imaging software at 34 GHz are in progress.

Also note that the observed solar disk is not flat due to errors in the optical system. This problem doesn't cause any serious problems for flare studies. However, it is necessary to correct the instrumental deformation of the disk component for structures which spatially extend over a few arcmin when a quantitative study is needed. This problem will be resolved before the next solar maximum.

### 2.2. Spectral Study

#### 23-Apr-98 X1.2 Flare

This GOES X1.2 class flare occurred at S13 E91. The maximum correlation coefficients of this flare at 17 and 34 GHz are 0.21 and  $8.0 \times 10^{-3}$ , respectively. Because the foot point emission is occulted by the solar limb, only loop top emission is observed in this event. This is a good example of a loop top source whose properties may be studied without interference by strong emission from footpoint sources.

Time profiles of 17 GHz and 34 GHz emissions and flare images are shown in Fig. 2a. The flux densities of radio sources at both frequencies reached 1500 sfu and 750 sfu at the peak time, respectively, and both profiles are very similar to each other. The spectral index derived from these profiles is also plotted in this figure ('+' mark). The spectral index is almost constant,  $\sim 1$  when the intensity is high, and it rapidly changes to almost zero after 05:48UT. It suggests that continuous acceleration of electrons lasted until this time and the accelerated electron were rapidly thermalized after that. Under assumption of uniform magnetic field strength and isotropic pitch-angle distribution, the spectral index of non-thermal electrons is  $\sim 2.5$  (Dulk 1985).

Grey colors in Figure 2 (b) and (c) show Stokes-I (upper panels) and Stokes-V (lower panels) images at 17 GHz at the peak and decay times. The 34 GHz map (white contours) and hard X ray map (Yohkoh HXT M1 band: 23-33 keV, black contours) are overlaid on the 17 GHz map (grey scale) in the upper panels. During the peak time, a large radio source at 17 GHz appeared at the loop top. The degree of polarization is less than 20 %. The position of the radio source is different from that of the hard X ray source. It seems that the M1 band (23—33 keV) image includes large contribution from thermal electron. In the decay time, the radio source elongated in the north-south direction and the north part is overlapped with the hard X-ray source. Judging from the flat spectrum, the 17 and 34 GHz sources are possibly of thermal origin.

Results of detailed analyses of this event are described by Sato and Hanaoka in this proceeding.

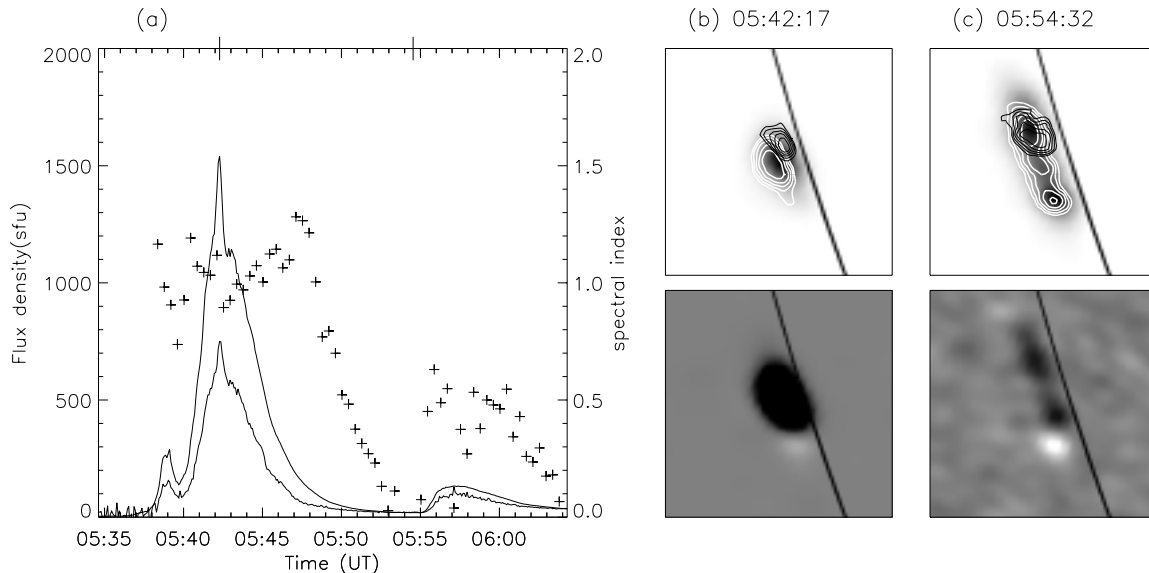


Fig. 2.. (a): Time profiles of 17 and 34 GHz flux densities and the microwave and mm-wave spectral index. (b) and (c): Flare images at the peak time and in the late phase, respectively. Grey scale, white contours, and black contours show images at 17 GHz, 34 GHz and HXT M1 band, respectively. The flux density at 34 GHz in (a) is multiplied by a factor of 3. Contour levels are 17.7, 25.0, 35.4, 50.0, 70.7 % of the peak brightness for each image. The field of view is 155 arc sec  $\times$  155 arcsec.

### 2.3. Timing Study

#### 02-May-98 C5.4 Flare

This flare is a GOES C5.4 class flare occurred at S20, E9. The maximum correlation coefficients at 17 and 34 GHz are  $1.7 \times 10^{-2}$  and  $5.6 \times 10^{-4}$ , respectively.

The flare images are shown in Fig. 3(c). Two microwave sources, i.e., the north and south sources, can be clearly seen. Time profiles of brightness temperatures and spectrum indices of the north and south sources are plotted in Fig. 3(a) and 3(b). The north and south sources are highly polarized in the initial phase with polarization degrees of more than 50% and -50%, respectively.

The time profiles of the brightness temperatures show different aspects between the two sources. The emission from the south source, which is a dominant component in total fluxes at both frequencies, varies gradually with time. The spectrum index changes from soft to hard. On the other hand, the emission from the north source shows a more spiky time variation than that from the south source. The spectral indices change among different peaks. The peak time at 34 GHz delayed  $\sim 5$  sec with respect to that at 17 GHz. The 17 GHz peaks also delayed a few sec with respect to the corresponding HXR peaks (not shown in the figure). If we assume that life times of energetic electrons in a flare loop are determined by Coulomb collisions, the time delays observed in this event can be explained by longer life times of higher energy electrons.

### 2.4. Prominence Eruption

Quiet structure such as a prominence is also obtained at both frequencies. But note that the image at 34 GHz is noisier than that at 17 GHz.

The event occurred on May 21, 1998. Before the eruption (the first column in fig. 4), almost the same structures are observed at both frequencies.

In the 17 GHz images, a helical structure of the prominence is resolved. On the other hand, such a structure is not resolved at 34 GHz in spite of better spatial resolution because the prominence at 34 GHz is not deconvolved since its brightness is lower than the confidence level in the imaging process (CLEAN). However, the expanding motion can be traced also at 34 GHz. The spectrum index estimated from flux densities shows an actual time variation. In the case where the source is unresolved the absolute value lacks accuracy but it is possible to know the tendency of its variation. After the start of the eruption, the brightness temperature at 34 GHz decreases more rapidly than

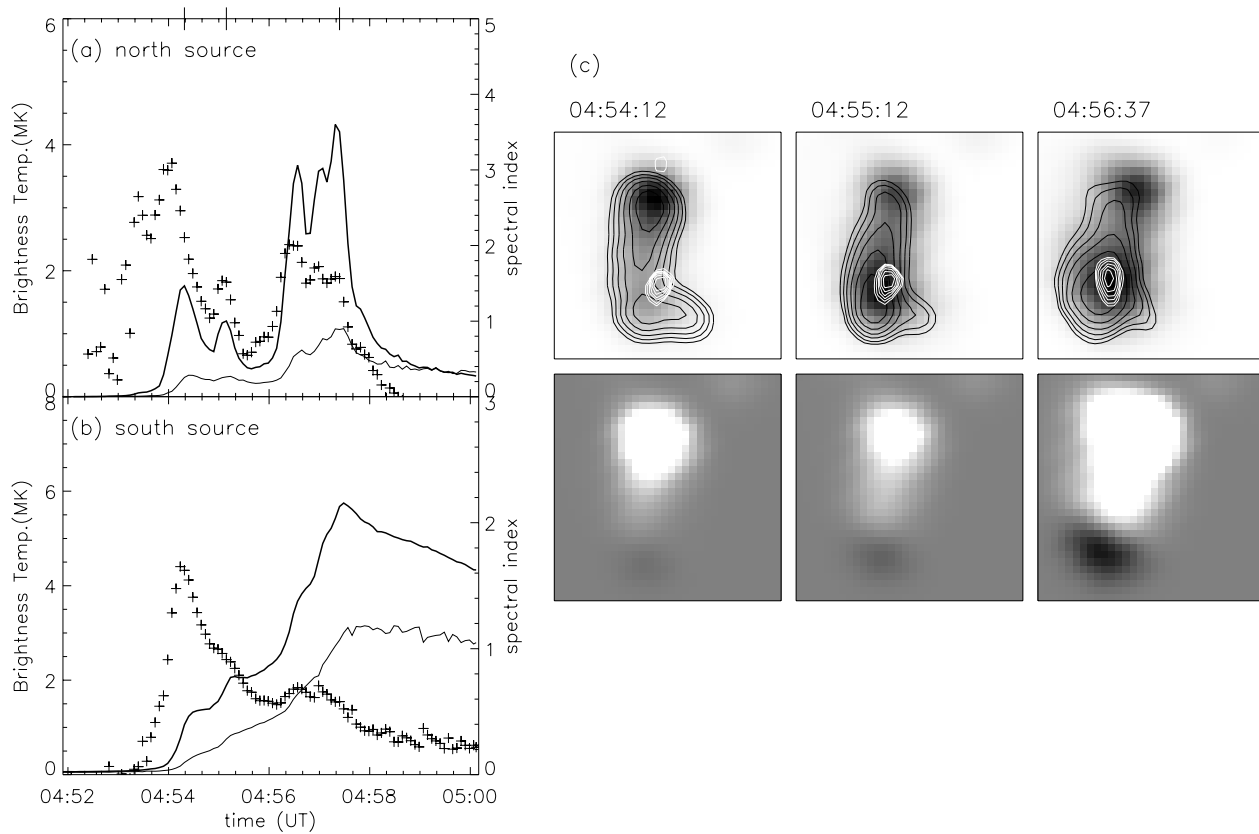


Fig. 3. Time profiles of brightness temperatures and spectral indices of the north source (a) and the south source (b), and images at several peaks (c). The grey scale images in the upper and lower panels show 17 GHz Stokes-I and -V maps, respectively. Black and white contours show brightness distributions at 34 GHz and HXT M2 band. Contour levels are 17.7, 25.0, 35.4, 50.0, 70.7 % of the peak brightness for each image. The field of view is 78 arcsec  $\times$  78 arcsec.

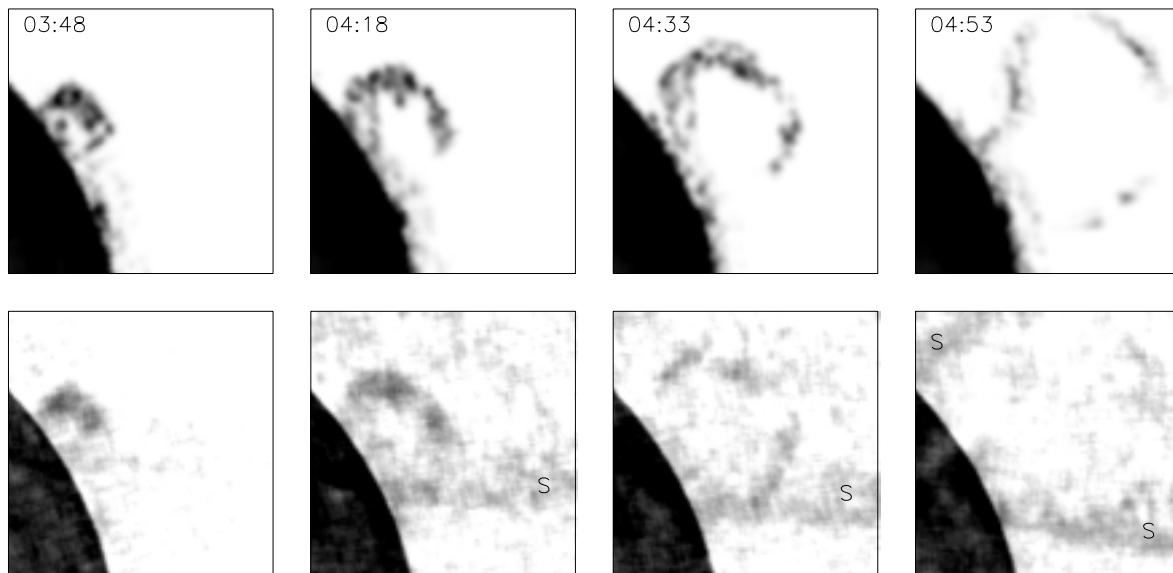


Fig. 4. Time evolution of an eruptive prominence. Upper and lower panels show 17 and 34 GHz images, respectively. A mark "S" denotes a sidelobe. The field of view is 10 arc min  $\times$  10 arc min.

that at 17 GHz. The prominence disappeared in the late phase (04:53 UT, the last panel) at 34 GHz. This suggests that the spectral index becomes steeper in the late phase. For free-free emission, the spectrum is flat in the case of optically thick plasma, and the power law index is -2 in the case of optically thin plasma. The present observation shows the time variation of the optical thickness of the eruptive prominence.

Large structures in 34 GHz images marked by “S” are sidelobes of the disk component.

### 3. Summary

A few tens of relatively strong flares, in which high quality 34 GHz images are expected to be obtained, have been observed since dual-frequency observation have started. Some of them are observed by other instruments such as *Yohkoh*. Preliminary analyses show that the combination of microwave, mm-wave and hard X-ray data provides us with information on a wide energy range of electrons accelerated or heated in solar flares. In addition, when more than two microwave and mm-wave sources appear, the spatially and temporally resolved spectral index provides crucial information for the emission mechanism of each source which is difficult to obtain from total flux observations.

It should be added that the time variation of the spectral index contains information on the generation and transportation of high energy electrons, and that high time resolution data from NoRH (100 msec) is quite useful for such a study when other data such as *Yohkoh* HXT and CGRO/BATSE are simultaneously used for comparison.

In the case of prominence eruptions or CME's, on the other hand, the time evolution of cool material can be traced using the NoRH. The optical thickness of the plasma can also be estimated. Combination of NoRH and data in other wavelengths such as  $H_{\alpha}$ , SOHO, etc, may compensate for poor spatial information of the NoRH.

A new frequency selective sub-reflector (FSS) is currently being developed to improve the optical system. It will allow us to obtain a high quality 34 GHz maps when the FSSs are replaced. I strongly hope that it will be finished before next solar maximum.

### References

- Dulk, G.A. 1985, *Ann. Rev. Astron. Astrophys.*, **23**, 169  
 Fujiki, K. 1997, Ph.D. Thesis  
 Koshiishi, H. 1996, Ph.D. Thesis  
 Kuseski, R.A. and P.N. Swanson, 1976, *Solar Physics*, **48**, 41  
 Linsky, J.L., 1973, *Solar Physics*, **28**, 409  
 Nakajima, H., M. Nishio, S. Enome, K. Shibasaki, T. Takano, Y. Hanaoka, C. Torii, H. Sekiguchi, T. Bushimata, S. Kawashima, N. Shinohara, Y. Irimajiri, H. Koshiishi, T. Kosugi, Y. Shiomi, M. Sawa and K. Kai 1994, *Proceeding of the IEEE*, **82**, No.5, 705-707  
 Takano, T., H. Nakajima, S. Enome, K. Shibasaki, M. Nishio, Y. Hanaoka, Y. Shiomi, H. Sekiguchi, S. Kawashima, T. Bushimata, N. Shinohara, C. Torii, K. Fujiki and Y. Irimajiri 1997, *Coronal Physics from Radio and Space Observations (Lecture Note in Physics)* 183  
 Zirin, H., B.M. Baumert and G.J. Hurford, 1991, *Astrophys. Journal.*, **370**, 779